

**ATTITUDE DETERMINATION SYSTEM FOR NANO SATELLITE USING
EXTENDED KALMAN FILTER ON ARM7TDMI PLATFORM**

by

ADAM AIN BIN MOHD POIN KEUI

**Thesis submitted in fulfilment of the requirements
for the degree of
Master of Science**

September 2014

ACKNOWLEDGMENTS

In the name of Allah, the most gracious and the most merciful. First and foremost I offer my sincerest gratitude to my supervisor, Professor Othman Sidek, who has guided and supported me with his patience and knowledge throughout my research. I attribute my accomplishment to his encouragement, patience, effort and without him this thesis would not have been completed. One simply could not wish for a better and friendlier supervisor as he is. His suggestions and advices had helped me in my times of despair when my research were facing some problems.

I also owe my sincerest gratitude to Professor Md Azlin Md Said as my co-supervisor who also helped me in the completion of my thesis. I would like to extend my gratitude to Mr Muhammad Fadly Nikmat for also guiding me in my research.

Many thanks to the staffs of Collaborative Microelectronic Design Excellence Center (CEDEC) who were involved directly or indirectly in this research work. My appreciation also goes to the School of Electrical and Electronic Engineering (SEEE), USM for giving me the opportunity to further my studies.

Finally, I would like to thank my parents who has been supporting me with their patience during the completion of my thesis. I would like to thanks Astronautics Technology Sdn. Bhd. (ATSB) and Malaysia Space Centre (ANGKASA) for giving me the opportunity to be involved with the InnoSAT satellite project.

TABLE OF CONTENTS

Acknowledgments	ii
Table of Contents	iii
List of Tables	vi
List of Figures	vii
List of Abbreviations	xi
List of Symbols	xv
Publication	xviii
Abstrak	xix
Abstract	xxi

CHAPTER 1 – INTRODUCTION

1.1 Background	1
1.2 Problem Statement	2
1.3 Objective of study	3
1.4 Scope and Limitations	4
1.5 Thesis Organization	4

CHAPTER 2 – OVERVIEW OF ATTITUDE DETERMINATION SYSTEM AND ARCHITECTURE

2.1 Introduction	5
2.2 Attitude Determination System Architectures	5
2.3 Satellite Orbit Description	9
2.3.1 Keplerian Orbit	9
2.3.2 Two-Line Element	13
2.3.3 Julian Date	14
2.3.4 Orbit Model	15

2.4	Attitude Representation	18
2.5	Coordinate Frames	23
2.5.1	Reference Coordinate Frame	23
2.5.2	Spacecraft Coordinate Frame	24
2.5.3	Earth Centered Inertial (ECI) to Earth Centered Earth Fixed (ECEF) rotation	25
2.6	Sun Model	26
2.6.1	Eclipse Model	28
2.7	International Geomagnetic Reference Field (IGRF) model	30
2.8	Extended Kalman Filter	31
2.9	Embedded system ARM7TDMI	36
2.9.1	Space Environment	38
2.10	ARM7TDMI Development Board	42
2.11	Summary	44

CHAPTER 3 – METHODOLOGY

3.1	Introduction	46
3.2	Attitude Determination System (ADS) Implementation on ARM7TDMI and ARM Interface software.....	47
3.3	Double Precision Floating-Point Format	58
3.4	ADS Simulation Overview	60
3.4.1	ADS Simulation Parameters	60
3.4.2	Satellite Toolkit (STK).....	62
3.5	Summary of Methodology	62

CHAPTER 4 – RESULT AND DISCUSSION

4.1	Performance of ARM7TDMI modeling algorithms	63
4.2	Performance of ARM7TDMI Extended Kalman filter (EKF).....	66

4.3	Computation Time Performance of ARM7TDMI	84
4.4	Summary of ARM7TDMI ADS Performance	85
CHAPTER 5 – CONCLUSIONS AND FUTURE WORK		
5.1	Conclusion	86
5.2	Future Work.....	86
References		88
APPENDICES		91
APPENDIX A – ARM7TDMI ADS SIMULATION PROCEDURE		92
APPENDIX B – ADS MAIN PROGRAM		95
APPENDIX C – ORBIT MODEL C PROGRAM		110
APPENDIX D – GREGORIAN TO JULIAN DATE CONVERSION C PROGRAM.....		113
APPENDIX E – IGRF MODEL C PROGRAM		114
APPENDIX F – SUN MODEL C PROGRAM		121
APPENDIX G – EKF C PROGRAM		123
APPENDIX H – GAUSS MATRIX INVERSION C PROGRAM		133
APPENDIX I – ARM INTERFACE SOFTWARE		135
I.1	VB 6.0 ARM Interface Software Description	135
I.2	Microsoft Visual Basic 6.0 Programming	135
APPENDIX J – ATTITUDE OUTPUT OF 2 INNOSAT ORBITS.....		146
APPENDIX K – INNOSAT EULER ANGLE EXTRACTED FROM STK		148

LIST OF TABLES

	Page
Table 2.1	Orbit shape relationship with eccentricity 10
Table 3.1	Sun and magnetic field vector components data format received by the ARM7TDMI 51
Table 3.2	Euler angles sent by ARM7TDMI 56
Table 3.3	InnoSAT structural parameters courtesy of Astronautics Technology Sdn. Bhd. (ATSB) 60
Table 3.4	InnoSAT TLE data courtesy of ATSB 60
Table 3.5	Initial InnoSAT attitude from STK simulation 61
Table 3.6	Simulation scenarios and EKF measurement covariances 61
Table 3.7	Initial EKF covariances 61
Table 4.1	InnoSAT orbital position determination comparison analysis to STK generated orbital positions 64
Table 4.2	InnoSAT magnetic field model output analysis to STK generated magnetic field vector 65
Table 4.3	InnoSAT sun position vector comparison analysis to STK generated sun position vector 65
Table 4.4	EKF and AR7TDMI accuracy analysis results in Scenario 1 71
Table 4.5	EKF and AR7TDMI accuracy analysis results in Scenario 2 74
Table 4.6	EKF and AR7TDMI accuracy analysis results in Scenario 3 76
Table 4.7	EKF and AR7TDMI accuracy analysis results in Scenario 4 79
Table 4.8	EKF and AR7TDMI accuracy analysis results in Scenario 5 81
Table 4.9	EKF and AR7TDMI accuracy analysis results in Scenario 6 84
Table 4.10	Execution time of ARM7TDMI microprocessor of EKF 84
Table 4.11	Execution speed of ARM7TDMI microprocessor of EKF 85

LIST OF FIGURES

	Page
Figure 2.1	AAUSAT-II overall satellite structure (Andresen et al., 2005) 6
Figure 2.2	AAUSAT overall satellite structure (Brand and Bakes, 2007) 7
Figure 2.3	Geometric properties of an elliptical orbit with the Earth as focal point 10
Figure 2.4	Keplerian orbital elements describing satellite orbit about the Earth 11
Figure 2.5	Relationship between True Anomaly and Eccentric Anomaly 12
Figure 2.6	Two Line Element (TLE) for ØRSTED (Krogh et al., 2002) 13
Figure 2.7	Argument of Latitude as the sum of Argument of Perigee and True Anomaly 17
Figure 2.8	Triad rotation of a rigid body satellite referring to a reference frame 18
Figure 2.9	Rotation about the third axis with angle Φ_a (Wertz, 1978) 20
Figure 2.10	The ECI and ECEF coordinate frame 23
Figure 2.11	Spacecraft Body Coordinate for InnoSAT satellite 24
Figure 2.12	Sunlight and eclipse determination diagram where satellite will in the eclipse region if it crosses the $R'_{sat,ECI}$ points (Andresen et al., 2005) 29
Figure 2.13	EKF Algorithm Flow Diagram 35
Figure 2.14	Embest S3CEV40 Development Board 43
Figure 2.15	Structure of Embest S3CEV40 Development Board Block Diagram (Embest Info and Tech Co. Ltd., 2001) 43
Figure 2.16	Embest Emulator for ARM JTAG 44
Figure 3.1	ADS setup 47
Figure 3.2	Summarized ADS software flow 48
Figure 3.3	Sensor data receiving flow of ARM7TDMI 50
Figure 3.4	Sensor data deciphering mode 52

Figure 3.5	Euler angles sending to ARM7TDMI via UART	56
Figure 3.6	Double and single precision floating-point format	59
Figure 3.7	InnoSAT orbit simulation using STK 10	62
Figure 4.1	InnoSAT orbit model orbital position determination in the ECI frame output compared to STK generated orbital position	64
Figure 4.2	Orbital position output error compared to STK generated orbital position	64
Figure 4.3	InnoSAT IGRF magnetic field vector determination in the ECI frame output compared to STK generated magnetic field vector	65
Figure 4.4	Magnetic field vector output error compared to STK generated magnetic field vector	65
Figure 4.5	InnoSAT sun model sun position vector determination in the ECI frame output compared to STK generated sun position vector	66
Figure 4.6	Sun position vector output error compared to STK generated sun position vector	66
Figure 4.7	Estimated roll state of InnoSAT satellite compared with STK roll in Scenario 1	67
Figure 4.8	Estimated pitch state of InnoSAT satellite compared with STK pitch in Scenario 1	67
Figure 4.9	Estimated yaw state of InnoSAT satellite compared with STK yaw in Scenario 1	67
Figure 4.10	Converging of estimated roll state of InnoSAT satellite to the true state in Scenario 1	68
Figure 4.11	Converging of estimated pitch state of InnoSAT satellite to the true state in Scenario 1	69
Figure 4.12	Converging of estimated yaw state of InnoSAT satellite to the true state in Scenario 1	69
Figure 4.13	Estimated roll error from STK roll in Scenario 1	70
Figure 4.14	Estimated pitch error from STK pitch in Scenario 1	70
Figure 4.15	Estimated yaw error from STK yaw in Scenario 1	70
Figure 4.16	Estimated roll state of InnoSAT satellite compared with STK roll in Scenario 2	71

Figure 4.17	Estimated pitch state of InnoSAT satellite compared with STK pitch in Scenario 2	72
Figure 4.18	Estimated yaw state of InnoSAT satellite compared with STK yaw in Scenario 2	72
Figure 4.19	Estimated roll error from STK roll in Scenario 2	73
Figure 4.20	Estimated pitch error from STK pitch in Scenario 2	73
Figure 4.21	Estimated yaw error from STK yaw in Scenario 2	73
Figure 4.22	Estimated roll state of InnoSAT satellite compared with STK roll in Scenario 3	74
Figure 4.23	Estimated pitch state of InnoSAT satellite compared with STK pitch in Scenario 3	74
Figure 4.24	Estimated yaw state of InnoSAT satellite compared with STK yaw in Scenario 3	75
Figure 4.25	Estimated roll error from STK roll in Scenario 3	75
Figure 4.26	Estimated pitch error from STK pitch in Scenario 3	76
Figure 4.27	Estimated yaw error from STK yaw in Scenario 3	76
Figure 4.28	Estimated roll state of InnoSAT satellite compared with STK roll in Scenario 4	77
Figure 4.29	Estimated pitch state of InnoSAT satellite compared with STK pitch in Scenario 4	77
Figure 4.30	Estimated yaw state of InnoSAT satellite compared with STK yaw in Scenario 4	77
Figure 4.31	Estimated roll error from STK roll in Scenario 4	78
Figure 4.32	Estimated pitch error from STK pitch in Scenario 4	78
Figure 4.33	Estimated yaw error from STK yaw in Scenario 4	78
Figure 4.34	Estimated roll state of InnoSAT satellite compared with STK roll in Scenario 5	79
Figure 4.35	Estimated pitch state of InnoSAT satellite compared with STK pitch in Scenario 5	79
Figure 4.36	Estimated yaw state of InnoSAT satellite compared with STK yaw in Scenario 5	80
Figure 4.37	Estimated roll error from STK roll in Scenario 5	80

Figure 4.38	Estimated pitch error from STK pitch in Scenario 5	81
Figure 4.39	Estimated yaw error from STK yaw in Scenario 5	81
Figure 4.40	Estimated roll state of InnoSAT satellite compared with STK roll in Scenario 6	82
Figure 4.41	Estimated pitch of InnoSAT satellite compared with STK pitch in Scenario 6	82
Figure 4.42	Estimated yaw of InnoSAT satellite compared with STK yaw in Scenario 6	82
Figure 4.43	Estimated roll error from STK roll in Scenario 6	83
Figure 4.44	Estimated pitch error from STK pitch in Scenario 6	83
Figure 4.45	Estimated yaw error from STK yaw in Scenario 6	83
Figure A.1	Setup of EMBEST S3CEV40 Development Board to PC	92
Figure A.2	EMBEST S3CEV40 Development Board components used	93
Figure I.1	ARM Interface Software descriptions	135

LIST OF ABBREVIATIONS

CF	Compact Flash
ACS	Attitude Control System
ADCS	Attitude Determination and Control System
ADC	Analog-to-Digital Converter
ADS	Attitude Determination System
ANGKASA	Malaysian National Space Agency
ATSB	Astronautics Technology Sdn. Bhd.
CHARM	CubeSat Hydrometric Atmospheric Radiometer Mission
CHIME	CubeSat Heliospheric Imaging Experiment
COTS	Commercial of The Shelf
DSP	Digital Signal Processor
DCM	Direction Cosine Matrix
DMA	Direct Memory Access
ECI	Earth Centered Inertial
ECEF	Earth Centered Earth Fixed
EKF	Extended Kalman filter
EPS	Electric Power Supply

ExEMFP Experimental Earth Magnetic Field Probe

ExPSS Experimental Pyramidal Sun Sensor

FIFO First In First Out

FPGA Field-Programmable Gate Array

GUI Graphical User Interface

I²C Inter-Integrated Circuit

I\O Input\Output

IP Intellectual Property

I²S Inter-Integrated Circuit Sound

IDE Intergrated Drive Electronics

IGRF International Geomagnetic Reference Field

JTAG Joint Test Action Group

LCD Liquid Crystal Display

LED light Emitting Diode

MCU Microprocessor

MSE Mean Squared Error

NASA National Aeronautics and Space Administration

NORAD North American Aerospace Defense Command

OBC On-Board Computer

PC	Personal Computer
PLL	Phase-locked loop
PWM	Pulse-width modulation
RISC	Reduced Instruction Set Computing
RTC	Real Time Clock
SBC	Spacecraft Body Coordinate
SEADS	Space Experimental Attitude Determination System
SEE	Single Event Effects
SEB	Single Event Burnout
SEGR	Single Event Gate Rupture
SEL	Single Event Latchup
SEU	Single Event Upset
SET	Single Event Transient
SIO	Serial Input\Output
SPSS	Solar Panel Sun Sensor
SRAM	static random-access memory
STK	Satellite Toolkit
TID	Total Ionization Dose
TLE	Two Line Element

UART Universal Asynchronous Receiver/Transmitter

USB Universal Serial Bus

USM Universiti Sains Malaysia

UTC Coordinated Universal Time

LIST OF SYMBOLS

\mathbf{A}	attitude matrix
a_s	semimajor axis
\mathbf{B}	magnetic field vector
$B_{n,m}$	contribution of spherical harmonics of n and m degrees
c_f	distance from the ellipse center to the ellipse focal point (Earth)
$\Delta(t)$	time difference between the epoch and the last perigee passage before epoch
ε	obliquity of the ecliptic plane
E_a	Eccentric Anomaly
e_s	eccentricity
n_{rev}	mean motion
$\hat{\mathbf{e}}$	rotation axis
i_s	inclination
JD_{now}	current reference Julian date
K_k	Kalman gain
lat	Argument of latitude
M_{Epoch}	Mean anomaly since epoch
M_{sun}	Sun mean anomaly

M_a Mean Anomaly

ν_s True Anomaly

ω_s Argument of Perigee

ω Earth angular velocity

p_{orb} orbital period

P_k^- priori covariance

P_k posteriori covariance

Φ rotation angle

ϕ Euler pitch angle

ψ Euler yaw angle

Ω_s Right Ascension of Ascending Node

R measurement covariance

r_{sat} distance of the satellite from Earth

$\mathbf{R}_{sat,ECI}$ position of the satellite in unit vector in the ECI frame

$R_3(\psi)$ rotation from ECI to ECEF frame

$\mathbf{R}_{sun,ECI}$ sun position in ECI plane

\mathbf{R}_S satellite position with respect to Earth

\mathbf{R}_{SC} sun position with respect to Earth

T_{se} time since epoch

θ Euler roll angle

Q process covariance

q_1 quaternion parameter 1

q_2 quaternion parameter 2

q_3 quaternion parameter 3

q_4 quaternion parameter 4

w_k white process noise

$x(t)$ system state vector

x_k linear system model

\hat{x}_k posteriori state

v_k white measurement noise

x discrete linear stochastic equation

\hat{x}_k^- priori state

V_{sun} sun position in ECI frame

z_k measurement vector

z_k linear measurement model

PUBLICATION

A. Ain Mohd Poin Keui, M. Fadly, O. Sidek and M. A. Md Said, "EKF Implementation on S3DEV40 for InnoSAT Attitude Determination System", *2011 IEEE Conference on Computer Applications and Industrial Electronics (ICCAIE 2011)*, (2011).

**SISTEM PENENTUAN KEDUDUKAN UNTUK SATELIT NANO
MENGUNAKAN PENAPISAN KALMAN LANJUTAN PADA PLATFORM
ARM7TDMI**

ABSTRAK

Penapisan Kalman Lanjutan (PKL) telah digunakan dengan jayanya di dalam misi satelit. Akan tetapi, jika dibandingkan dengan kaedah penentuan kedudukan lain yang telah dihasilkan, ia adalah salah satu daripada algoritma yang memiliki komputasi yang paling berat dan dengan perkembangan terkini yang menggunakan satelit nano yang mempunyai kuasa elektrik, berat, ruang dan biasanya peruntukan yang terhad, adalah menjadi satu keutamaan untuk merekabentuk sebuah Sistem Penentuan Kedudukan (SPK) yang dapat mematuhi kekangan ini. Maka, penambakan dari segi komputasi dibuat kepada projek InnoSAT dengan menggantikan mikropengawal RCM3400 dengan mikropemproses berasaskan ARM7TDMI untuk menguji kebolehan ARM7TDMI. ARM7TDMI telah dipilih kerana ia merupakan antara mikropemproses yang dikenali dan digunakan dalam kebanyakan peralatan elektronik kerana kerendahan kuasanya dan kerana ia tahan lasak. Papan pembangunan EMBEST S3CEV40 yang digunakan dilengkapi dengan S3C44B0X yang merupakan mikropemproses ARM7TDMI. Ujian dijalankan dengan menghubungkan papan pembangunan kepada komputer peribadi yang telah dipasang dengan perisian antara muka ARM yang di program berdasarkan Visual Basic 6.0. Papan pembangunan telah dibenamkan dengan perisian SPK berdasarkan PKL. Komunikasi antara kedua-dua sistem adalah

menggunakan komunikasi 3-wayar bersiri. Perisian antara muka ARM akan bertindak sebagai penerima satelit dengan menghantar data penerima melalui komunikasi bersiri. Data penerima yang diterima of papan pembangunan ARM7TDMI digunakan untuk menghitung kedudukan satelit. Setelah menghitung, papan pembangunan ARM7TDMI akan menghantar kembali data kepada komputer peribadi untuk penyimpanan dan analisis lanjutan. Penyimpanan data ini dijalankan oleh perisian antara muka ARM. Ini adalah untuk mensimulasi SPK untuk menerima data penerima, menghitung dan menghantar kembali data kedudukan kepada sistem Pengendalian Data Atas Papan (PDAP) yang dilakukan untuk 2 orbit satelit. Hasil pemodelan orbit satelit dan elemen yang diukur iaitu arah matahari dan medan magnet adalah sesuai untuk dijadikan input kepada PKL. PKL menunjukkan hasil yang memberangsangkan kerana sisihan piawai kedudukan satelit untuk setiap paksi adalah kurang dari 3° mengatasi toleransi 5° yang diperlukan. Penambahbaikan yang diperlukan adalah penambaan kepada komputasi yang memerlukan 3 saat untuk setiap komputasi SPK.

ATTITUDE DETERMINATION SYSTEM FOR NANO SATELLITE USING EXTENDED KALMAN FILTER ON ARM7TDMI PLATFORM

ABSTRACT

Extended Kalman Filter (EKF) has been successfully utilized in satellites missions. However, in comparison to other attitude determination methods developed, it is one of the most computationally burdening algorithm and with the new development of using nano satellites which have limited electrical power, mass, space and usually budget, it is essential to design an Attitude Determination System (ADS) which conforms to this limitation. Therefore, in this thesis, as a computational improvement on the InnoSAT project, the RCM3400 microcontroller of the ADS is replaced with the ARM7TDMI based microprocessor to test its capability. The ARM7TDMI has been chosen since it is one of the well-known microprocessor used in various electronic equipment because it is low power and robust. The EMBEST S3CEV40 Development Board used, houses the S3C44B0X microprocessor which is an ARM7TDMI microprocessor. The testing is done by connecting the development board to a personal computer which has been installed with the ARM Interface Software based on Visual Basic 6.0. The development board is embedded with the ADS software based on the EKF. The communication for the two system uses 3-wire serial communication. The ARM Interface software will act as the sensor of the satellite by sending sensor data via serial communication. Sensor data received by the ARM7TDMI development board is used to calculate the attitude of the satellite. Once calculated, the ARM7TDMI development

board will send attitude data back to the PC for storage and further analysis. Data storage is done by ARM Interface software. This is to simulate the ADS system to receive sensor data, calculate and send back attitude data to On Board Data Handling (OBDH) system which is done for 2 satellite orbits. Modelling results of satellite orbit and sensed elements consisting of sun position and magnetic field are suitable to be used for EKF input. The EKF shows promising results as the satellite attitude standard deviation in each axis is less than 3° exceeding the 5° required tolerance. The only improvement required is the computation which need 3 seconds for each computation on ADS.

CHAPTER 1

INTRODUCTION

1.1 Background

InnoSAT satellite program is a satellite program lead by Astronautics Technology Sdn. Bhd. (ATSB) and Malaysian National Space Agency (ANGKASA). InnoSAT is a $300 \times 100 \times 100 \text{mm}^3$ or a 3 unit CubeSat nanosatellite design. CubeSat was collaboratively designed by California Polytechnic State University and Stanford University's Space Systems Development Laboratory (Lee et al., 2009) to provide a standard design for picosatellite to reduce cost and development time, increase accessibility to space, and sustain frequent launches. Many institutions use this platform as their platform for various mission. Some like the Danish AAUSAT-II uses the CubeSat satellite platform for educational purposes and at the same time for research in gamma radiation in space (Andresen et al., 2005). California Institute of Technology and National Aeronautics and Space Administration (NASA) teamed up to design the CubeSat Hydrometric Atmospheric Radiometer Mission (CHARM) satellite to be used for Earth radiometry study which replaces the use of large and costly satellites (Lim et al., 2012). Dickinson et al. (2011) uses the CubeSat platform for their satellite to predict and diagnose space weather events at Earth. Many researches have been done using the CubeSat platform which is why the CubeSat is a suitable start off for InnoSAT as a new satellite research in Malaysia. The program provides local universities with the opportunity to be involved with a real satellite project with ATSB as the project leader as each university takes part by developing a specific subsystem for InnoSAT.

1.2 Problem Statement

Universiti Sains Malaysia (USM) was given the opportunity to develop the Attitude Determination System (ADS) of InnoSAT. ADS is one of the crucial subsystems of a satellite. The satellite would be flying blindly and eventually out of control without this subsystem. Thus USM took the opportunity to develop an ADS which has been designated Space Experimental Attitude Determination System (SEADS) and a Rabbit RCM3400 based microcontroller board which process sensor measurement to generate InnoSAT attitude. SEADS consists of three sensors which has been installed on InnoSAT. First sensor consists of 4 sets of three sided pyramidal sun sensors designated Experimental Pyramidal Sun Sensor (ExPSS), second is a magnetometer designated Experimental Earth Magnetic Field Probe (ExEMFP) and finally a redundant sun sensor designated Solar Panel Sun Sensor (SPSS) which utilizes InnoSAT solar panels to generate sun vector. All sensors provide sun position and magnetic field vector of InnoSAT in Spacecraft Body Coordinate (SBC) frame.

Readings from the sensors are to be processed by the Rabbit RCM3400 microcontroller board to be stored in an on board flash memory and to generate attitude of InnoSAT. The Rabbit RCM3400 controller board has been embedded with an attitude determination algorithm consisting of Kepler orbit model which generates InnoSAT position vector in Earth Centered Inertial (ECI) frame, Keplerian sun model and International Geomagnetic Reference Field (IGRF) model which generates the sun and magnetic field vectors respectively in the ECI frame and a combination of Extended Kalman filter (EKF) and Q-method which calculate InnoSAT attitude using both sun and magnetic field vector in ECI and SBC frames.

Though, this was the plan for RCM3400 controller board, a combination of issues surfaced during the implementation of the algorithm which are improper Julian date representation, RCM3400 computation speed limit and memory burden of ADS. The first issue is the Julian date. Julian date is a crucial initial parameter to the orbit model where the orbit model is a crucial starting point for further attitude determination processing. However, during implementation of attitude determination methods in Attitude Determination and Control System (ADCS) of InnoSAT, it is found that the RCM3400 cannot represent Julian date variable accurately in 32 bits(floating point) but should be represented in double 64 bit numbers, because the date precision exceed the 32 bit decimal limit causing major calculation errors. Another issue is the computation speed limitation and memory burden of ADS on RCM3400 micro-controller. The EKF with the inverse of element matrix larger than 3×3 and the IGRF calculation with an order of 10 caused a significant overloading of RCM3400 memory and reduction in processing time.

Therefore, in order to improve on the capabilities of InnoSAT ADS, an ARM7TDMI microprocessor will be tested to see whether the capabilities of the ARM7TDMI would be suitable for InnoSAT ADS.

1.3 Objective of study

From above, the objectives of this research are

- (i) To estimate the attitude of InnoSAT from combination of two position sensors using EKF

- (ii) To embed the EKF attitude estimation algorithm in the ARM7TDMI based microprocessor
- (iii) To compare the performance and result of the experimentation of the real time embedded EKF with Satellite Toolkit (STK) software.

1.4 Scope and Limitations

The scope of this research is limited to the ADS of InnoSAT only. Though a real satellite would include a control system, which completes the ADCS of a full satellite, adding the control system to the research would be too big for this research. Testing would only be done to the microprocessor by using a development board on ground. Sensor readings are simulated readings from STK by using proposed InnoSAT Two Line Element (TLE) provided by ATSB.

1.5 Thesis Organization

This thesis is divided into 5 chapters which entails the implementation EKF based ADS on ARM7TDMI. Chapter 1 introduces InnoSAT which is the satellite platform and base for this research. Research goals and overview is also included in this chapter. Chapter 2 presents a literature review of ADS used by various groups around the world. The fundamentals of ADS and EKF are also explained in this section as well space requirement of a satellite system. Chapter 3 presents the method of experimentation for the implementation of the EKF on the ARM7TDMI microprocessor. Chapter 4 discusses the results of the implementation of the EKF based ADS on the ARM7TDMI microprocessor. Finally, Chapter 5 concludes the finding of this thesis and the recommendations for future work.

CHAPTER 2

OVERVIEW OF ATTITUDE DETERMINATION SYSTEM AND ARCHITECTURE

2.1 Introduction

Attitude of a spacecraft is its orientation in space. Attitude determination is the process of computing the orientation of the spacecraft relative to either an inertial reference or some object of interest, such as Earth. This typically involves several types of sensors on each spacecraft and sophisticated data processing procedures (Wertz, 1978).

2.2 Attitude Determination System Architectures

Satellite subsystems are unique to one another. This is also true for the ADS. The configuration and combination of sensors and the built in electronic system depends on the mission, satellite size and shape.

One of the example is the Danish AAUSAT-II. It is a $10 \times 10 \times 10\text{cm}^3$ CubeSat weighting no more than 1kg . The satellite ADS hardware consists of three single axis rate gyro and a 3-axis magnetometer. The sampling of sensor measurement is done by an Atmel AT89C51 Microprocessor (MCU). The ADS which is the EKF calculations of AAUSAT-II is placed in the On-Board Computer (OBC) since the OBC is relatively powerful. The overall AAUSAT-II structure can be seen in Figure 2.1 (Andresen et al., 2005).

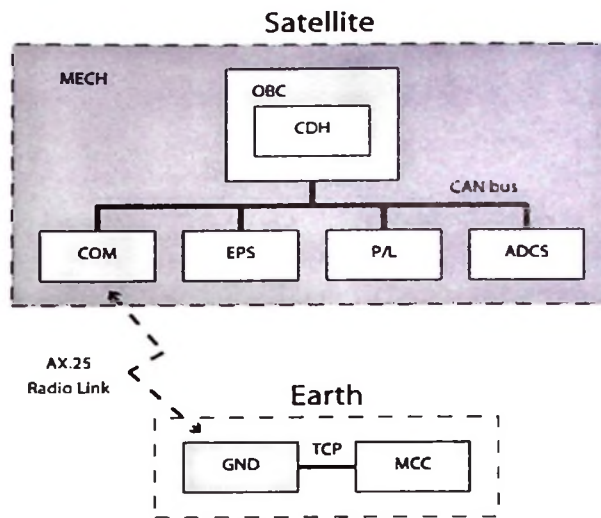


Figure 2.1: AAUSAT-II overall satellite structure (Andresen et al., 2005)

AAUSAT-II is the next generation of the Danish satellite AAUSAT. AAUSAT has the same dimension as AAUSAT-II and the ADCS architecture is as seen in Figure 2.2. A PIC16C774 microcontroller from Microchip was selected for the ADCS. The microcontroller had to sample data from three sample types, send sensor data to the OBC via Inter-Integrated Circuit (I²C) bus, interface actuators and execute control algorithms (Krogh et al., 2002). Software developed for the PIC16C774 microcontroller is mainly for data sampling from sensors and to control the satellite. The ADS algorithm is implemented on the OBC of the satellite.

Another work done by Brand and Bakes (2007) took a general look at nanosatellite OBC. The authors considered various processing cores for a $30\text{cm} \times 30\text{cm} \times 20\text{cm}$ nanosatellite and finally concluded that an AT91SAM7A2 ARM7 based processor from Atmel was the best processor for a nanosatellite OBC. The ARM-based processor was chosen since ARM processors are proven reliable because it has been used in a lot of handheld devices (Brand and Bakes, 2007). Eventhough the ARM processor is a reliable processor for various handheld devices, the space environment poses a totally

different threat to a satellite when compared with the Earth's environment. Brand and Bakes's main concern are errors caused by radiation exposure in the space since the chosen processor is not a space qualified component. However, in recent years, satellite developers has begun experimenting and using Commercial of The Shelf (COTS) components which include processors as well. Eventhough these COTS components are susceptible to radiation errors, they are much cheaper compared to space qualified components. Brand and Bakes (2007)'s also suggest that the vital part which is the onboard memory the satellite should consists only of static random-access memory (SRAM) and flash memory only with the inclusion of some form of detection and correction hardware. According to the authors as well, the most computationally complex operation a nanosatellite would have to deal with using its limited hardware is the IGRF modelling of ADCS. This confirms the high computation of the IGRF modelling.

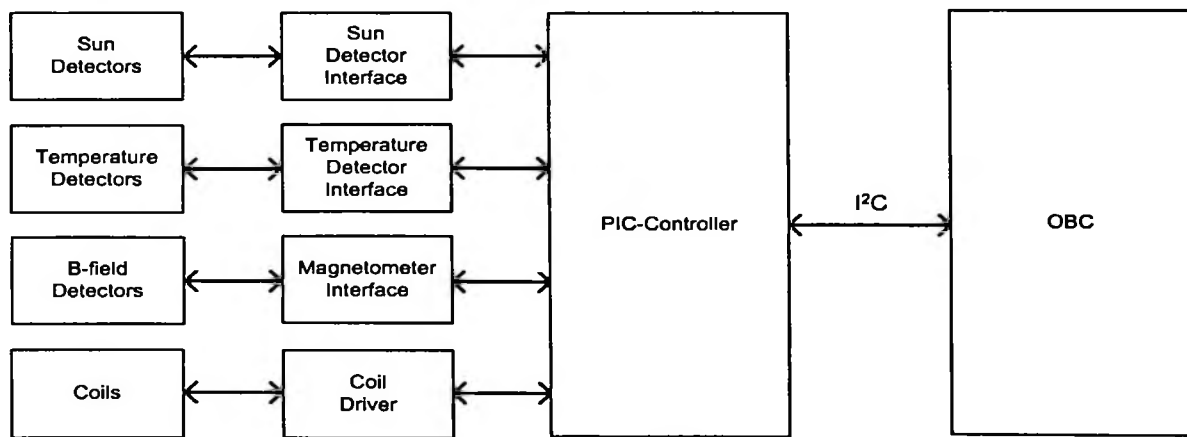


Figure 2.2: AAUSAT overall satellite structure (Brand and Bakes, 2007)

nCUBE is a Norwegian student satellite (Ose, 2004). It is in the same league as both AAUSAT satellite in terms of size and weight. The ADS or the attitude estimator also uses an EKF which is written in C programming language. The nCUBE team

chose an ATmega128L since it is the low power version. Ose (2004) also realized that EKF requires highly accurate variables, therefore the variables of the EKF in AAUSAT program is implemented as floating variables which has a range of $\pm 3.403 \times 10^{308}$ and an accuracy of $\pm 1.175 \times 10^{-308}$ (IEEE Std 754-2008, 2008; 754-1985, 1985). This also indicates the ATmega128L microcontroller is able to use variables in double precision format.

The CubeSat Heliospheric Imaging Experiment (CHIME) satellite as mentioned by Dickinson et al. (2011) uses a Gumstix Verdex computer for its OBC which also govern the attitude determination and control of CHIME. The CHIME satellite uses two sun sensors to determine its attitude.

Another architecture done by Ali et al. (2014) into the AraMiS-C1 satellite, is the integration of the Electric Power Supply (EPS) and the ADCS onto a single Cubesat standard tile. The AraMiS-C1 satellite system uses COTS components. Sensors on board consists of sun detector and magnetometer. System management of the satellite is done by a commercial MSP430F5438A ultra power 16-bit Reduced Instruction Set Computing (RISC) architecture microcontroller which support up to 25Mhz system clock.

Yang et al. (2012) used a TMS320C54 series Digital Signal Processor (DSP) from Texas Instruments to perform the duty of controller by implementing sampling, computing and actuating algorithms. The system performs a dual-vector attitude determination based on solar and Earth-magnetic sensor reading. The ADCS manages to stabilize the satellite the attitude with Earth-pointing precision of 5° *irc* when the sun in

visible.

2.3 Satellite Orbit Description

A satellite orbiting the Earth is considered a two point mass which are influenced by their mutual gravitational attraction (Jensen et al., 2010). This system can be described by using Kepler's three empirical laws of planetary motion (Wertz, 1978).

2.3.1 Keplerian Orbit

An orbit can be described using the method developed by Johannes Kepler which gives a description of the orbit size, shape and orientation, as well a spacecraft's position (Sellers et al., 2003). The method requires only 6 orbital elements which are:

- Semimajor axis, a_s
- Eccentricity, e_s
- Inclination, i_s
- Right Ascension of Ascending Node (Ω_s)
- Argument of Perigee, ω_s
- True Anomaly, v_s

A size and shape of an orbit is defined respectively by the semimajor axis, a_s and eccentricity, e_s . From Sellers et al. (2003), the eccentricity is given by

$$e_s = \frac{c_f}{a_s} \quad (2.1)$$

where c_f is the distance from the ellipse center to the ellipse focal point (Earth) as in Figure 2.3.

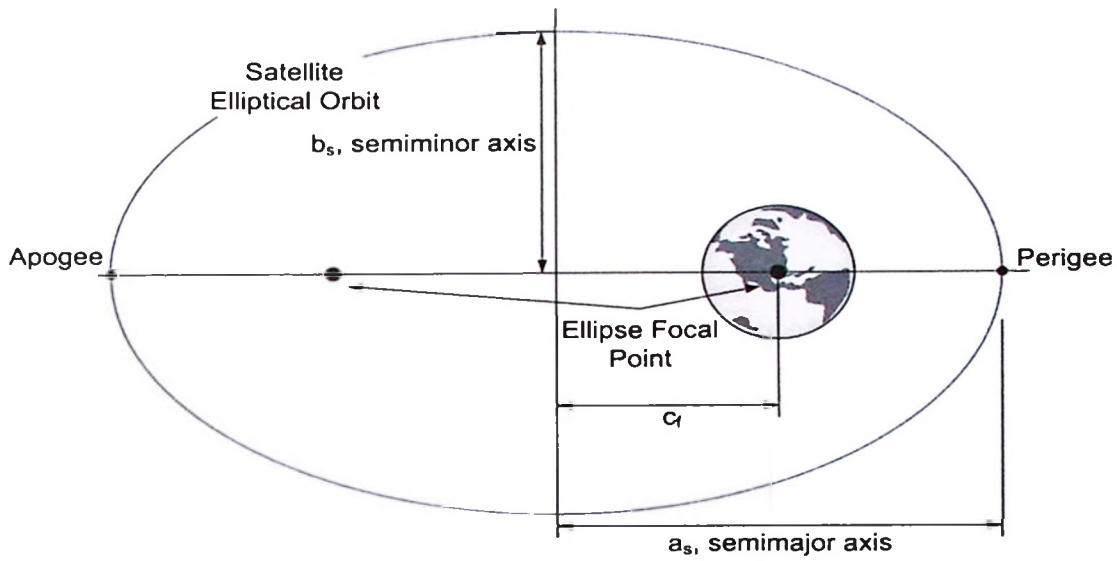


Figure 2.3: Geometric properties of an elliptical orbit with the Earth as focal point

The shape of the orbit either a circle, ellipse, parabola or a hyperbola depends on the eccentricity, e_s and the relationship can be seen in Table 2.1.

Table 2.1: Orbit shape relationship with eccentricity

Orbit Shape	Eccentricity
Circle	$e_s = 0$
Ellipse	$0 < e_s < 1$
Parabola	$e_s = 1$
Hyperbola	$e_s > 1$

The orbit plane orientation is determined by two elements which are inclination and right ascension of ascending node as in Figure 2.4.

The inclination, i_s is the angle between orbit plane and the Earth's equatorial plane as seen in Figure 2.4. If $i_s = 0^\circ$, the orbit is Equatorial orbit and if $i_s = 90^\circ$ it becomes a Polar orbit. Orbits in between the two values are prograde orbits and when the $i_s > 90^\circ$

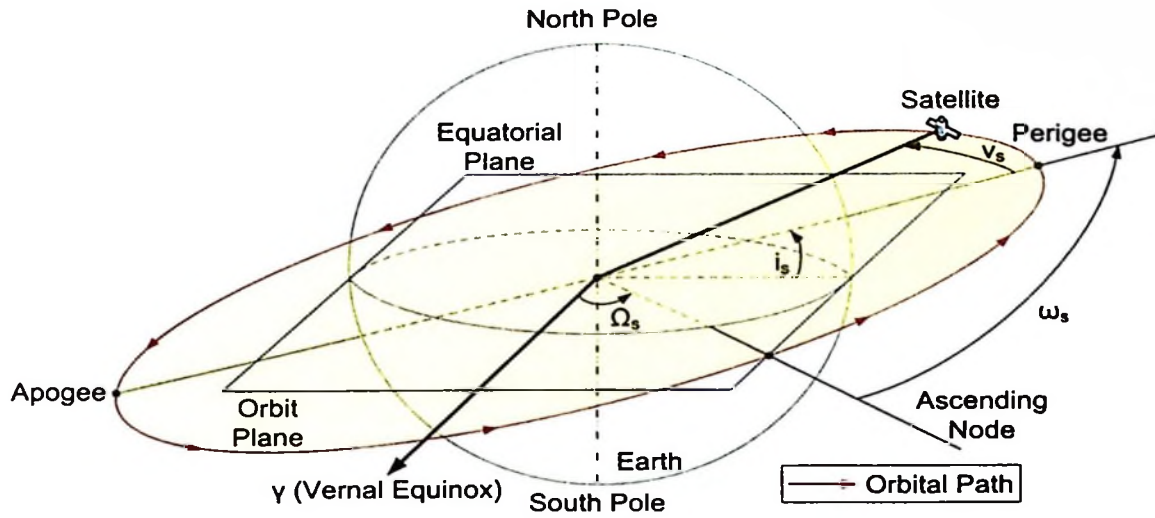


Figure 2.4: Keplerian orbital elements describing satellite orbit about the Earth

the satellite orbits in reverse also known as retrograde orbit (Sellers et al., 2003).

As seen from Figure 2.4, Ω_s , is the angle measured from the Vernal Equinox to the ascending node which is the point at which the satellite crosses the equator plane going from south to north.

The argument of perigee, ω_s as in Figure 2.4, determines the orientation of orbit in the plane. It is the angle measured in the satellite's direction of motion from the ascending node to the perigee. Perigee is the closest approach to the satellite to the Earth.

True anomaly, v_s will be calculated from the mean anomaly, M_a . Mean anomaly, M_a is an angle with no physical meaning but mathematically it represents the angle of satellites position in its orbital path given by,

$$M_a = 360 \cdot \left(\frac{\Delta(t_e)}{p_{orb}} \right) [deg] \quad (2.2)$$

where:

$\Delta(t_e)$ is the time difference between the epoch and the last perigee passage before epoch and p_{orb} is the orbital period.

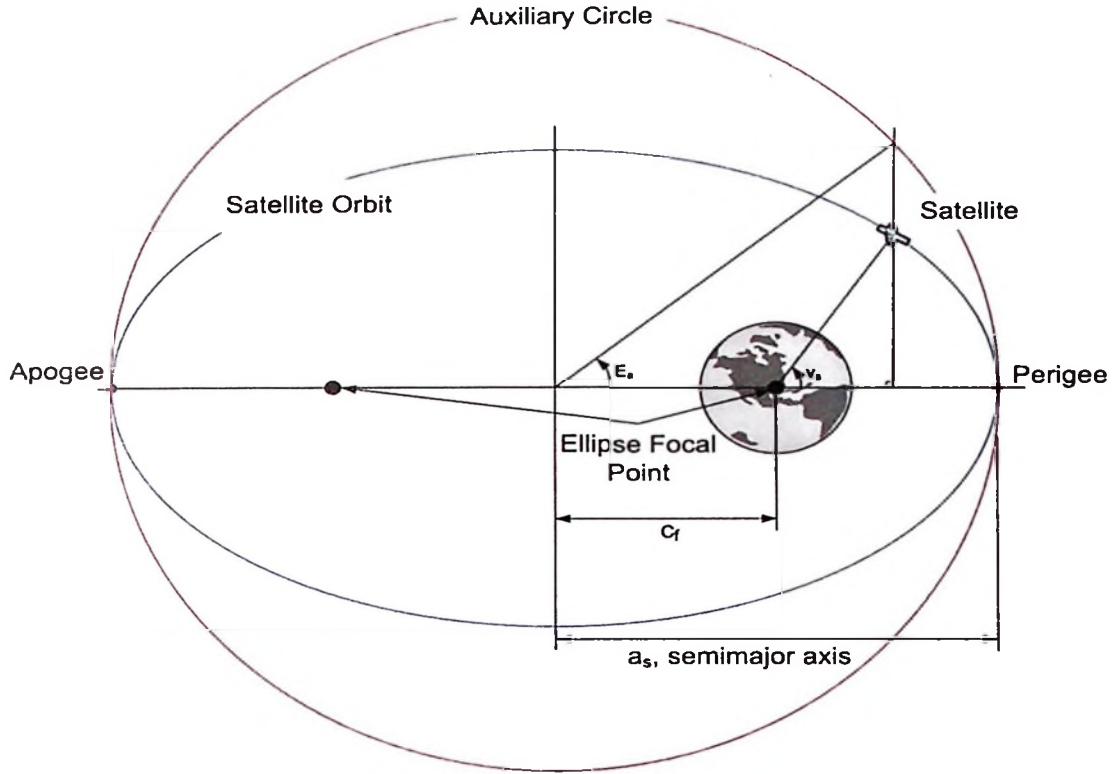


Figure 2.5: Relationship between True Anomaly and Eccentric Anomaly

Mean anomaly is linked to the true anomaly by an intermediate variable, the Eccentric anomaly, E_a which can be seen in Figure 2.5. The mean and eccentric anomalies are related by Kepler's equation as

$$M_a = E_a - e_s \sin E_a \quad (2.3)$$

Then Gauss's equation relates the eccentric anomaly to the True Anomaly, v_s by

$$\tan\left(\frac{v_s}{2}\right) = \left(\frac{1+e_s}{1-e_s}\right)^{1/2} \tan\left(\frac{E_s}{2}\right) \quad (2.4)$$

From Equation 2.4, True Anomaly, v_s can be expressed directly as a function of Mean Anomaly, M_a by expanding in a power series in orbital Eccentricity, e_s to yield

$$v_s = M_a + 2e_s \sin(M_a) + 5e_s^2 \frac{\sin(2M_a)}{4} \quad (2.5)$$

2.3.2 Two-Line Element

TLE or short for two-line element is a simple data format of two line sets having 69 characters which describes the orbit of an Earth satellite. This general perturbation element sets is available for all space objects and is maintained by North American Aerospace Defense Command (NORAD). An example of a TLE format is as seen in Figure 2.6 (Krogh et al., 2002).

Satellite Name	Satellite Number	International Designator	Epoch Year & Julian Day Fraction	1 st Derivative Of Mean Motion	2 nd Derivative of Mean Motion	Drag Term	Ephemeris Type	Element Number and Check Sum
ØRSTED	1 25635U	990088B	02191.70184970	000001847	00000000	47904-3	0	6051
	2 25635	96.4606	180.7500 0147084	145.9562	215.1160	14.44218556	169104	
	Satellite Number	Inclination	Right Ascension of ascending node	Eccentricity	Argument of Perigee	Mean Anomaly	Mean Motion in Revolutions per day	Revolution number at Epoch and Check Sum

Figure 2.6: TLE for ØRSTED (Krogh et al., 2002)

Other than the orbital parameters explained previously in Section 2.3.1, the TLE includes other following parameters:

Time of Epoch: This represents the time when the orbital parameters were ob-

tained. Epoch year is described in the first two numbers. The remaining numbers in the integral part is the Julian day and the fraction represent the fractional portion of the day.

1st Derivative of Mean Motion: This represents the change in the mean motion of the satellite. It is the half value of the mean motion in revolutions per day squared and is caused by atmospheric drag pulling a satellite into a lower orbit and accelerates it downward towards the Earth.

2nd Derivative of Mean Motion: This term is the 2nd second derivative of the mean motion divided by six, in units of revolutions per day cubed and is usually set to zero since it is not used because the orbit model only considers the force of Earth's gravity acting on the satellite for estimation.

Drag Term: A drag term or radiation pressure coefficient consists of a coefficient describing the effect of drag on a satellite. It is based on a satellite surface and mass.

Mean Motion: Mean motion describes the number of revolution a satellite completes in day.

Revolution Number at Epoch: This parameter gives the number of orbit at the Epoch time when TLE was taken.

2.3.3 Julian Date

A very useful and common representation of time which simplifies astronomical calculation and satellite orbit propagation is the Julian date. It is counted in day plus a

fraction of the day beginning at noon universal time. It has been counted in days since 1st of January 4713 BC at noon universal time (Wertz, 1978; Danby, 1988; Sinnott, 1991).

The Julian date used in this research will not use the entire Julian date from 1st January 4713BC noon but instead will use the Julian date starting from noon UTC on the 1st January 2000. This will offset the Julian date by 2451545 days subtracted from the ordinary Julian date.

2.3.4 Orbit Model

Having known the orbit of a satellite, at a certain point and time from a TLE, it is also required to determine the position and motion of a satellite in order to determine the attitude of a satellite. A simple two body Keplerian orbit propagator model developed by the AAUSAT team will be used (Krogh et al., 2002). This orbit model will use the orbital and time parameters from a given TLE.

The first step of the orbit model is to determine the current mean anomaly of the satellites orbital position. The time since epoch, T_{se} is used here. It is the current time in Julian date minus the Julian date at Epoch given in the TLE. The current Mean Anomaly, M_a is calculated in degrees using Equation 2.6, which includes mean anomaly at epoch, M_{Epoch} and the mean motion, n_{rev} from the TLE.

$$M_a = M_{Epoch} + 360n_{rev}T_{se} \quad (2.6)$$

The semi major axis, a_s which represent the largest radius of an eccentric orbit as shown in Figure 2.3 is given by

$$a_s = \left(\frac{m_g}{\left(\frac{2n_{rev}\pi}{86400} \right)^2} \right)^{1/3} \quad (2.7)$$

Next the daily changes of Argument of Perigee, $\dot{\omega}_s$ and daily changes of the Right Ascension of Ascending Node, $\dot{\Omega}_s$ is determined since the Argument of Perigee, ω_s and Ω_s changes with a constant speed relative to the ECI frame is determined. Parameters used in the determination are orbital Inclination, i_s , the orbital Eccentricity, e_s , Semi Major Axis of the orbit, a_s and the Earth's Equatorial Radius, r_{earth} (Krogh et al., 2002; Wertz, 1978).

$$\dot{\omega}_s = 4.98204 \left(\left(\frac{r_{earth}}{a_s} \right)^{3.5} \right) (5 \cos(i_s)^2 - 1) ((1 - e_s^2)^2)^{-1} \quad (2.8)$$

$$\dot{\Omega}_s = 9.9641 \left(\left(\frac{r_{earth}}{a_s} \right)^{3.5} \right) \cos(i_s) ((1 - e_s^2)^2)^{-1} \quad (2.9)$$

Accordingly the current Argument of Perigee, ω_s and the Ω_s can now be determined by updating the same parameters given in the TLE parameters, $\omega_{s,TLE}$ and $\Omega_{s,TLE}$ with $\dot{\omega}_s$ and $\dot{\Omega}_s$ resulting in

$$\omega_s = \omega_{s,TLE} + T_{se} \dot{\omega}_s \quad (2.10)$$

$$\Omega_s = \Omega_{s,TLE} - T_{se}\dot{\Omega}_s \quad (2.11)$$

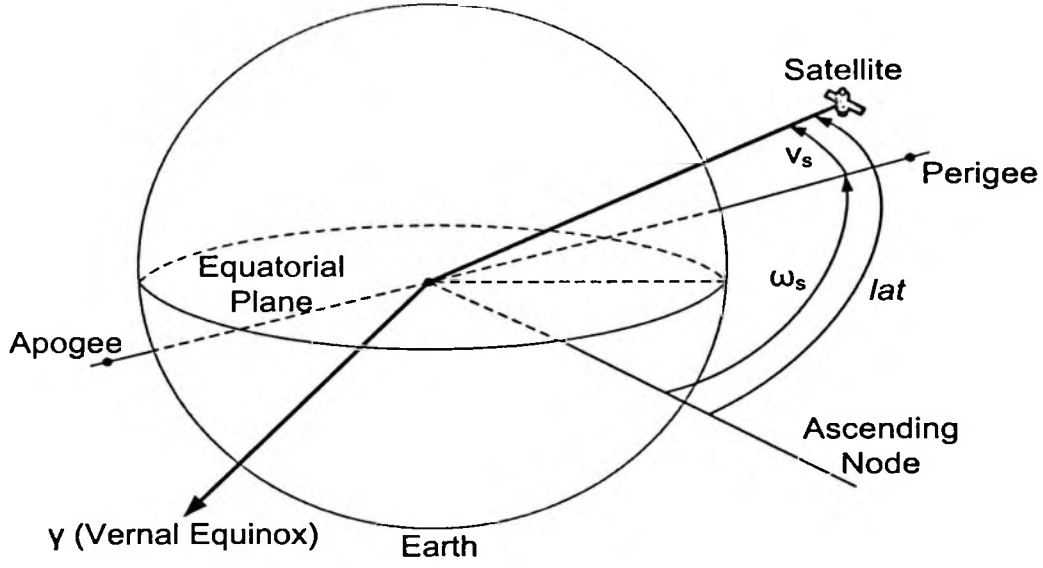


Figure 2.7: Argument of Latitude as the sum of Argument of Perigee and True Anomaly

After that, the Argument of Latitude, lat is determined. It represents the angle between the ascending node and the current satellite position with respect to the center of the Earth or in the ECI frame as seen in Figure 2.7. The angle is actually the sum of Argument of Perigee, ω_s and the True Anomaly, v_s from Equation 2.5 thus producing

$$lat = \omega_s + v_s \quad (2.12)$$

Using the Argument of Latitude, lat , Right Ascension of Ascending Node, Ω_s and the satellite orbital inclination, i_s , the position of the satellite in unit vector in the ECI frame is determined by

$$\begin{aligned}
x_{sat} &= \cos(lat) \cos(\Omega_s) - \sin(lat) \sin(\Omega_s) \cos(i_s) \\
y_{sat} &= \cos(lat) \sin(\Omega_s) + \sin(lat) \cos(\Omega_s) \cos(i_s) \\
z_{sat} &= \sin(lat) \sin(i_s)
\end{aligned} \tag{2.13}$$

To give a measurable figure to the orbital position of the satellite position in kilometers, the position vector in Equation 2.13 is multiplied with the radius of the satellites orbital position, r_{sat} (in kilometers) as below

$$r_{sat} = a_s \frac{1 - e_s^2}{1 + e_s \cos(v_s)} \tag{2.14}$$

2.4 Attitude Representation

Rotation of reference frames expresses the orientation of a rigid body satellite, relative to some reference coordinate frame for example reference frames from Figure 2.10. The fundamental quantity specifying the orientation of a satellite is the Direction Cosine Matrix (DCM). Referring to Figure 2.8, the orthogonal, satellite right handed

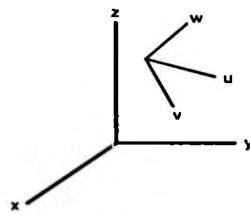


Figure 2.8: Triad rotation of a rigid body satellite referring to a reference frame

triad "uvw" is in the vicinity of the reference frame "xyz". Thus the satellite triad \hat{u} , \hat{v} and \hat{w} can be specified and fixed to the reference coordinate frame which creates a 3x3 matrix having 9 parameters. This 3x3 matrix is known as the, attitude matrix, \mathbf{A} which

is

$$\mathbf{A} \equiv \begin{bmatrix} u_x & u_y & u_z \\ v_x & v_y & v_z \\ w_x & w_y & w_z \end{bmatrix} \quad (2.15)$$

with $\hat{\mathbf{u}} = (u_x, u_y, u_z)^T$, $\hat{\mathbf{v}} = (v_x, v_y, v_z)^T$ and $\hat{\mathbf{w}} = (w_x, w_y, w_z)^T$. Each of the elements is a cosine of the angle between a body unit vector and a reference axis. For example, the cosine of the angle between $\hat{\mathbf{v}}$ and reference y-axis is represented by v_y . Due to this, \mathbf{A} is referred to as DCM.

A DCM is a coordinate transformation (Wertz, 1978) that maps vectors from a reference frame to the body frame where if \mathbf{a} is a vector with components a_1 , a_2 and a_3 along the reference axes, then

$$\mathbf{A}\mathbf{a} = \begin{bmatrix} u_x & u_y & u_z \\ v_x & v_y & v_z \\ w_x & w_y & w_z \end{bmatrix} \begin{bmatrix} a_1 \\ a_2 \\ a_3 \end{bmatrix} = \begin{bmatrix} \hat{\mathbf{u}} \cdot \mathbf{a} \\ \hat{\mathbf{v}} \cdot \mathbf{a} \\ \hat{\mathbf{w}} \cdot \mathbf{a} \end{bmatrix} \equiv \begin{bmatrix} a_u \\ a_v \\ a_w \end{bmatrix} \quad (2.16)$$

The components of $\mathbf{A}\mathbf{a}$ are the components of the vector \mathbf{a} along the body triad $\hat{\mathbf{u}}$, $\hat{\mathbf{v}}$, and $\hat{\mathbf{w}}$. Other than the DCM, there are other parameterizations that specifies the orientation of a rigid. However, in this thesis, the Euler angles and the Euler Symmetric Parameters normally known as quaternion are used. The Euler axis/angle (Wertz, 1978) based on the right-hand rule is a simple anti-clockwise rotation in the positive sense of the third axis by the angle, Φ_a as in Figure 2.9. The DCM for this rotation is given by

$$A_3(\Phi_a) = \begin{bmatrix} \cos \Phi_a & \sin \Phi_a & 0 \\ -\sin \Phi_a & \cos \Phi_a & 0 \\ 0 & 0 & 1 \end{bmatrix} \quad (2.17)$$

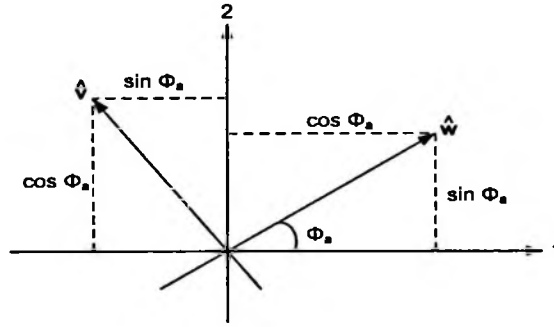


Figure 2.9: Rotation about the third axis with angle Φ_a (Wertz, 1978)

The DCM rotation in the first and second axis by the angle, Φ_a is represented by $A_1(\Phi_a)$ and $A_2(\Phi_a)$, respectively and they are

$$A_1(\Phi_a) = \begin{bmatrix} 1 & 0 & 0 \\ 0 & \cos \Phi_a & \sin \Phi_a \\ 0 & -\sin \Phi_a & \cos \Phi_a \end{bmatrix} \quad (2.18)$$

$$A_2(\Phi_a) = \begin{bmatrix} \cos \Phi_a & 0 & -\sin \Phi_a \\ 0 & 1 & 0 \\ \sin \Phi_a & 0 & \cos \Phi_a \end{bmatrix} \quad (2.19)$$

All three matrices have the trace

$$\text{tr}(A(\Phi_a)) = 1 + 2 \cos \Phi_a \quad (2.20)$$

The trace of a DCM representing a rotation by an angle, Φ_a about an arbitrary axis takes the same value. Generally, the axis rotation from one reference frame to another reference frame might not be one of the 'xyz' orthogonal axes but might be a unit vector, \hat{e} and an angle of rotation, Φ_a which results with a general DCM as

$$A = \begin{bmatrix} \cos \Phi_a + e_1^2(1 - \cos \Phi_a) & e_1 e_2(1 - \cos \Phi_a) + e_3 \sin \Phi_a & e_1 e_3(1 - \cos \Phi_a) - e_2 \sin \Phi_a \\ e_1 e_2(1 - \cos \Phi_a) - e_3 \sin \Phi_a & \cos \Phi_a + e_2^2(1 - \cos \Phi_a) & e_2 e_3(1 - \cos \Phi_a) + e_1 \sin \Phi_a \\ e_1 e_3(1 - \cos \Phi_a) + e_2 \sin \Phi_a & e_2 e_3(1 - \cos \Phi_a) - e_1 \sin \Phi_a & \cos \Phi_a + e_3^2(1 - \cos \Phi_a) \end{bmatrix} \quad (2.21)$$

(Wertz, 1978)

Using the same principal with a unit vector along rotation axis, \hat{e} and an angle of rotation, Φ_a a set of four parameters known as the Euler symmetric parameter or quaternion can be introduced to represent rotation of a rigid body and they are(Wertz, 1978)

$$q_1 \equiv e_1 \sin \frac{\Phi_a}{2} \quad (2.22)$$

$$q_2 \equiv e_2 \sin \frac{\Phi_a}{2} \quad (2.23)$$

$$q_3 \equiv e_3 \sin \frac{\Phi_a}{2} \quad (2.24)$$

$$q_4 \equiv \cos \frac{\Phi_a}{2} \quad (2.25)$$

These four parameters are not independent but satisfy the constraint equation (Wertz, 1978)

$$q_1^2 + q_2^2 + q_3^2 + q_4^2 = 1 \quad (2.26)$$

The quaternion DCM is given by

$$A(q) = \begin{bmatrix} q_1^2 - q_2^2 - q_3^2 + q_4^2 & 2(q_1q_2 + q_3q_4) & 2(q_1q_3 - q_2q_4) \\ 2(q_1q_2 - q_3q_4) & -q_1^2 + q_2^2 - q_3^2 + q_4^2 & 2(q_2q_3 + q_1q_4) \\ 2(q_1q_3 + q_2q_4) & 2(q_2q_3 - q_1q_4) & -q_1^2 - q_2^2 + q_3^2 + q_4^2 \end{bmatrix} \quad (2.27)$$

Quaternion is widely used because there are only four simple parameters for consideration and it is less burdening on the processor because the expression for the quaternion DCM does not involve trigonometric functions which require extensive computing. Eventhough the quaternion performs better at rigid body rotations, another type of rotation has more apparent geometrical significance of a rotation which known as the Euler angles (Wertz, 1978). Euler angles are usually used for analysis to find closed form solutions to the equation of motion in special cases particularly for small angle of rotations. Contrary to quaternion, Euler angles use three sets of rotation angle commonly known roll, pitch and yaw. For a satellite attitude, the angles rotates to the SBC frame about a given axis (Ose, 2004). The roll angle, θ rotates about the SBC frame x-axis, pitch angle, ϕ rotates about the SBC frame y-axis and finally, the yaw angle, ψ rotates about the SBC frame z-axis.

Since Euler angles provide better physical representation of attitude and the quaternion is useful for calculation (Wertz, 1978), the quaternion can be rotated using (Wertz, 1978)

$$\begin{bmatrix} \phi \\ \theta \\ \psi \end{bmatrix} = \begin{bmatrix} \arctan\left(\frac{2(q_1q_4 + q_2q_3)}{1 - 2(q_1^2 + q_2^2)}\right) \\ \arctan(2(q_4q_2 - q_1q_3)) \\ \arctan\left(\frac{2(q_3q_4 + q_2q_1)}{1 - 2(q_2^2 + q_3^2)}\right) \end{bmatrix} \quad (2.28)$$

2.5 Coordinate Frames

This section describes the frames used for determining the attitude in three dimensional space. The frames are important as the points on a rigid body is different depending on different coordinate frames thus the correct reference frame has to be known in all conditions. The method to rotate from the ECI frame to the Earth Centered Earth Fixed (ECEF) frame is also introduced in this section.

2.5.1 Reference Coordinate Frame

Since InnoSAT orbits the Earth, two specific Earth related coordinate system will be used. They are the ECI and ECEF coordinate frame which have their origin in the geographical center of Earth as shown in Figure 2.10.

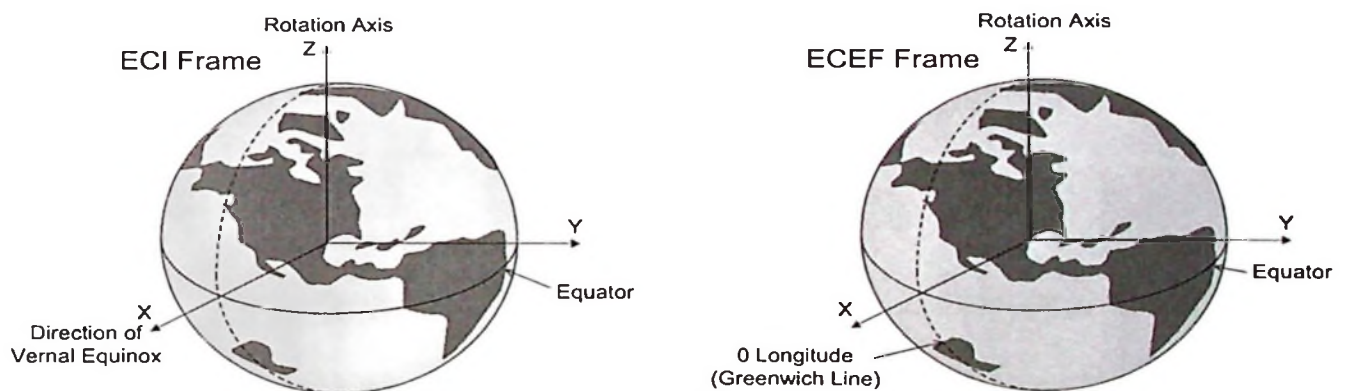


Figure 2.10: The ECI and ECEF coordinate frame

The first coordinate frame, Earth Centered Inertial represents a coordinate system with its origin in the center of Earth and is fixed relative to the Earth rotation. The X-axis is parallel to the direction of Vernal Equinox. The Vernal Equinox is the point where the plane of the Earth's orbit about the Sun, crosses the equator going from

South to North. The Z-axis is parallel to the Earth's rotational axis.

The second Earth coordinate frame, the Earth Centered Earth Fixed frame has a similar origin and Z-axis as the ECI frame but with a different X-axis. The X-axis, stays and intersect the zero longitude of Earth designated the Greenwich Meridian which fixes the ECEF frame to Earth thus, the system rotates with it.

2.5.2 Spacecraft Coordinate Frame

The satellite itself requires a set of fixed coordinate frames for attitude determination of the satellite. The attitude and position of the satellite is accordingly given as a rotation between the satellite fixed coordinate frames and reference frames.

First is the SBC which is placed in the center of mass of the satellite and fixed to the satellite geometric axes. The axis representation can be seen in Figure 2.11.

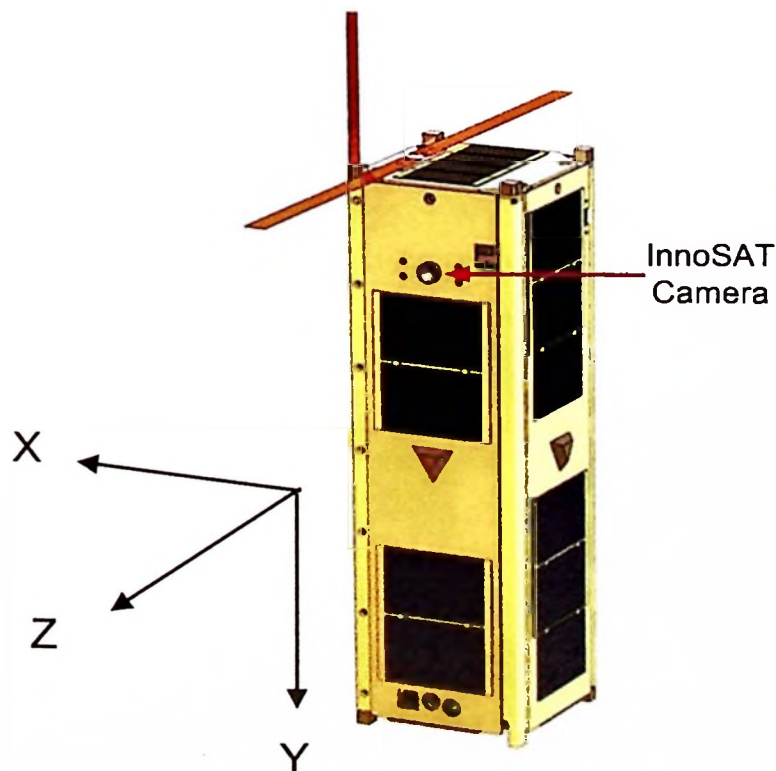


Figure 2.11: Spacecraft Body Coordinate for InnoSAT satellite